Volume 2 | Number 12 | 28 March 2014 | Pages 2097–2284

Journal of Materials Chemistry C

Materials for optical and electronic devices

www.rsc.org/MaterialsC

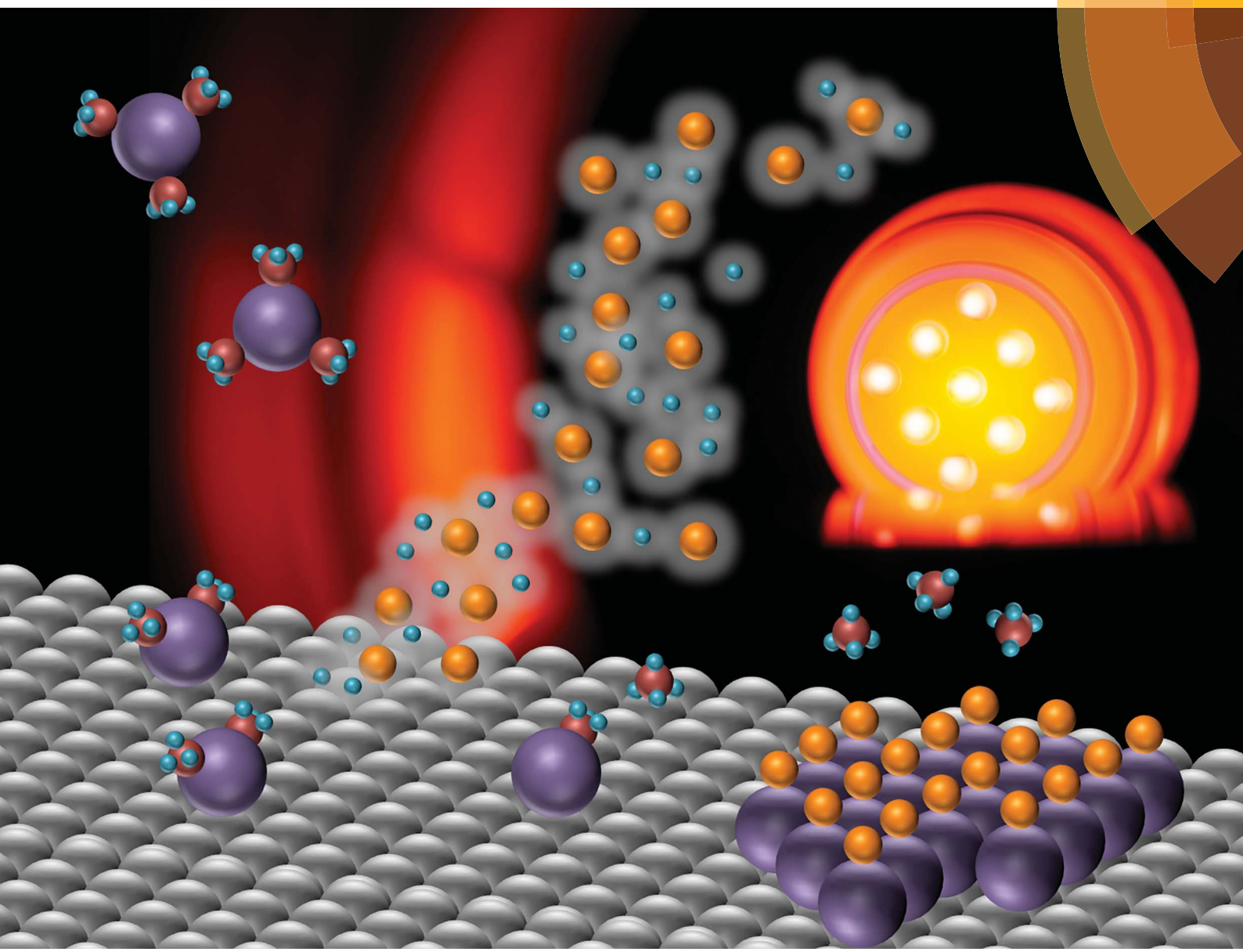

ISSN 2050-7526

ROYAL SOCIETY OF CHEMISTRY

PAPER

Cagla Ozgit-Akgun, Necmi Biyikli *et al.*

Hollow cathode plasma-assisted atomic layer deposition of crystalline AlN, GaN and $Al_xGa_{1-x}N$ thin films at low temperatures

Journal of Materials Chemistry C

PAPER

Cite this: J. Mater. Chem. C, 2014, 2, 2123

Hollow cathode plasma-assisted atomic layer deposition of crystalline AlN, GaN and $Al_xGa_{1-x}N$ thin films at low temperatures

Cagla Ozgit-Akgun,*[ab] Eda Goldenberg,[a] Ali Kemal Okyay[abc] and Necmi Biyikli*[ab]

The authors report on the use of hollow cathode plasma for low-temperature plasma-assisted atomic layer deposition (PA-ALD) of crystalline AlN, GaN and $Al_xGa_{1-x}N$ thin films with low impurity concentrations. Depositions were carried out at 200 °C using trimethylmetal precursors and NH_3 or N_2/H_2 plasma. X-ray photoelectron spectroscopy showed the presence of 2.5–3 at.% O in AlN and 1.5–1.7 at.% O in GaN films deposited using NH_3 and N_2/H_2 plasma, respectively. No C impurities were detected within the films. Secondary ion mass spectroscopy analyses performed on the films deposited using NH_3 plasma revealed the presence of O, C (both <1 at.%), and H impurities. GIXRD patterns indicated polycrystalline thin films with wurtzite crystal structure. Hollow cathode PA-ALD parameters were optimized for AlN and GaN thin films using N_2/H_2 plasma. Trimethylmetal and N_2/H_2 saturation curves evidenced the self-limiting growth of AlN and GaN at 200 °C. AlN exhibited linear growth with a growth per cycle (GPC) of ~1.0 Å. For GaN, the GPC decreased with the increasing number of deposition cycles, indicating substrate-enhanced growth. The GPC calculated from a 900-cycle GaN deposition was 0.22 Å. Ellipsometric spectra of the samples were modeled using the Cauchy dispersion function, from which the refractive indices of 59.2 nm thick AlN and 20.1 nm thick GaN thin films were determined to be 1.94 and 2.17 at 632 nm, respectively. Spectral transmission measurements of AlN, GaN and $Al_xGa_{1-x}N$ thin films grown on double side polished sapphire substrates revealed near-ideal visible transparency with minimal absorption. Optical band edge values of the $Al_xGa_{1-x}N$ films shifted to lower wavelengths with the increasing Al content, indicating the tunability of band edge values with the alloy composition.

Received 7th December 2013
Accepted 7th January 2014

DOI: 10.1039/c3tc32418d

www.rsc.org/MaterialsC

Introduction

In the last few decades, considerable research has been devoted to the growth and characterization of III-nitride compound semiconductors (AlN, GaN, and InN) and their alloys, which emerged as versatile and high-performance materials for a wide range of electronic and optoelectronic device applications. Wurtzite type III-nitrides exhibit direct band gaps, which extend from the ultra-violet (UV) to the mid-IR spectrum with values of 6.2, 3.4 and 0.64 eV for AlN, GaN, and InN, respectively.[1,2] This feature allows the band gap of any ternary or quaternary III-nitride alloy to be easily tuned within the specified limits to adjust to a particular application. Metalorganic chemical vapor deposition (MOCVD)[3,4] and molecular beam epitaxy (MBE)[5] have already been proven to be successful techniques for achieving high-quality epitaxial III-nitride layers with low impurity concentrations and decent electrical properties. However, both of these methods employ high growth temperatures, which is neither compatible with the existing CMOS technology nor suitable for temperature-sensitive device layers (*e.g.* In-rich $In_xGa_{1-x}N$) and substrates (*e.g.* glass, flexible polymers, *etc.*). This incompatibility necessitates the development of alternative low-temperature processes for the deposition of III-nitride thin films and their alloys.

Atomic layer deposition (ALD) is a low-temperature material growth method, which is based on self-terminating surface reactions.[6] Unlike chemical vapor deposition (CVD), in ALD, precursors are pulsed into the reactor one at a time, separated by purging and/or evacuation periods. Unless decomposition occurs, precursor molecules do not tend to react with themselves and hence the reaction terminates when all the available reactive surface sites are occupied. This special growth mechanism is termed as "self-limiting" and results in highly uniform and conformal thin films, whose thicknesses can be controlled at the sub-angstrom scale. This makes ALD a powerful method especially for depositing films on nanostructured templates,[7–9] which is considered as a successful approach for improving the efficiency and/or sensitivity of devices through surface area

[a]UNAM – National Nanotechnology Research Center, Bilkent University, Ankara, 06800, Turkey. E-mail: ozgit@bilkent.edu.tr; biyikli@unam.bilkent.edu.tr; Fax: +90 (312) 266 4365; Tel: +90 (312) 290 3556

[b]Institute of Materials Science and Nanotechnology, Bilkent University, Ankara, 06800, Turkey

[c]Department of Electrical and Electronics Engineering, Bilkent University, Ankara, 06800, Turkey

enhancement. Moreover, alloy thin films can be easily deposited using ALD, either by controlling the relative vapor pressures of the precursors which are being pulsed into the reactor simultaneously during one of the half-cycles, or by designing a cycle that consists of subcycles of the constituent materials. The latter, which is generally named as "digital alloying", is a unique and facile route for obtaining alloy thin films with well-defined compositions.

Thermal ALD of AlN has been extensively studied using ammonia (NH_3) and various Al precursors: aluminum trichloride ($AlCl_3$),[10] dimethylethylamine alane ($Me_2EtN{:}AlH_3$),[11] triethylaluminum ($AlEt_3$),[12] trimethylaluminum ($AlMe_3$),[13] trimethylamine alane ($Me_3N{:}AlH_3$)[14] (with deuterated ammonia (ND_3)), and tris(dimethylamido)aluminum ($Al_2(NMe_2)_6$).[15] Plasma- and UV-assisted ALD of AlN have also been reported for $AlCl_3$–NH_3/H_2,[16,17] $AlMe_3$–NH_3 (ref. 18 and 19) and $AlMe_3$–N_2/H_2 (ref. 20) combinations. Although $AlCl_3$ is a highly reactive and thermally stable precursor, which yields good results in terms of achieving true ALD conditions, the use of halogenated precursors is in general not preferred due to several reasons. Most importantly, their reaction with hydrogen-containing nonmetals results in gaseous corrosive by-products (HCl in the case of chloride precursors), which can etch the deposited film, as well as the reactor components. Furthermore, halide ligands incorporate into the growing film and remain as impurities. They also create a memory effect in the chamber; *i.e.* residual halides in the system contaminate the subsequently deposited films for a long period of time following the use of a halogenated precursor. Among all the metalorganic Al precursors listed above, $AlMe_3$ is probably the most recognized one due to the well-known $AlMe_3$–H_2O thermal ALD process that is designed for depositing dielectric Al_2O_3 layers.[6] Unfortunately, thermal ALD of AlN using $AlMe_3$ and NH_3 is not possible since these two precursors only react at temperatures where $AlMe_3$ self-decomposition occurs.[13] Therefore, true ALD conditions for the deposition of AlN using $AlMe_3$ and NH_3 can only be achieved if the deposition temperature is lowered by enhancing the reactivity of NH_3 using an external energy source, such as plasma. Plasma-assisted ALD (PA-ALD) of nitride thin films is not limited by the use of NH_3; alternatively, a mixture of N_2 and H_2 gases can also be employed to create similar plasma radicals. Recently, our group reported on the PA-ALD of polycrystalline wurtzite AlN thin films at temperatures ranging from 100–500 °C.[21–23] Films deposited at temperatures within the ALD window (100–200 °C for both NH_3 and N_2/H_2 processes) were C-free and had low O concentrations (<3 at.%) despite the fact that 5N-grade plasma gases were used without any further purification. It is worth noting that the number of publications focusing on the PA-ALD (or plasma-assisted atomic layer epitaxy, PA-ALE) of AlN using $AlMe_3$ has increased considerably in the last few years.[24–28] AlN films deposited using PA-ALD were reported to be either amorphous or polycrystalline.[24–27] In a very recent study, Nepal *et al.*[28] demonstrated the PA-ALE of AlN films at 200–650 °C using $AlMe_3$ and N_2 plasma, and emphasized the significance of *ex situ* and *in situ* surface pretreatments for obtaining epitaxial thin films. PA-ALD and -ALE grown AlN thin films were used in memristors,[29] transistors,[30–33] and in other devices for work function tuning[34] and passivation.[35–37]

When compared to AlN, a significantly less number of publications concentrated on the ALD of GaN thin films. Thermal and plasma-assisted ALE, as well as thermal ALD of GaN have been studied at temperatures >450 °C using triethylgallium ($GaEt_3$),[38] trimethylgallium ($GaMe_3$),[39,40] and gallium trichloride ($GaCl_3$)[41,42] precursors. Lower ALE growth temperatures (350–400 °C) were achieved when gallium chloride (GaCl) was used as the Ga precursor.[43] Sumakeris *et al.*[44] used a novel reactor design that employs hot filaments to decompose NH_3 and deposited epitaxial GaN films using $GaEt_3$ within the temperature range of 150–650 °C. Recently, Sharp *et al.*[45] presented their results on the PA-ALD of GaN thin films using $GaEt_3$ and N_2/H_2 plasma. In their study, the concentrations of O and C impurities in GaN films were reported to be ≥3 at.%. Our initial efforts for depositing GaN thin films using $GaEt_3$ or $GaMe_3$ with NH_3 plasma resulted in amorphous thin films with high O concentrations (~20 at.%).[46,47] Although – at first – the most probable source of this contamination was presumed as the O-containing impurities in the 5N-grade NH_3 gas, subsequent experiments revealed the true source as the quartz tube of the inductively coupled plasma source itself. Such plasma-related oxygen contamination was also reported for GaN thin films grown by remote plasma enhanced CVD.[48] In view of these circumstances, the choice of N-containing plasma gas (N_2, N_2/H_2 or NH_3) determined the severity of O incorporation into AlN and GaN films deposited by PA-ALD.[49] We were able to deposit polycrystalline wurtzite GaN thin films with 4.7 at.% O and 4.2 at.% C impurities using the $GaMe_3$–N_2/H_2 PA-ALD process at 200 °C. As an effort to completely avoid this contamination problem, we replaced the original quartz-based inductively coupled RF-plasma (ICP) source of the ALD system with a stainless steel hollow cathode plasma (HCP) source,[50] which has been recently used for the deposition of epitaxial GaN thin films by migration enhanced afterglow.[51]

Here, we report on the low-temperature hollow cathode PA-ALD (HCPA-ALD) of crystalline AlN, GaN and $Al_xGa_{1-x}N$ thin films with low impurity concentrations. To the best of our knowledge, this is the first study reporting on the integration of HCP and ALD, as well as the first low-temperature self-limiting growth of crystalline $Al_xGa_{1-x}N$ thin films. Materials characterization efforts including structural, chemical, surface, and optical analyses are presented in detail.

Experimental details

Hollow cathode plasma-assisted atomic layer deposition

AlN, GaN and $Al_xGa_{1-x}N$ thin films were deposited at 200 °C in a modified Fiji F200-LL ALD reactor (Ultratech/Cambridge NanoTech Inc.), which is backed by an Edwards nXDS20iC dry scroll vacuum pump. In this modified configuration, the original quartz-based ICP source of the ALD system was replaced with a stainless steel HCP source (Meaglow Ltd.). The original RF power supply (Seren IPS Inc., R301), matching network controller (Seren IPS Inc., MC2) and automatic matching

network (Seren IPS Inc., AT-3) units were used to activate the HCP discharge. Prior to depositions, Si (100), Si (111), and *c*-plane sapphire substrates were cleaned by sequential ultrasonic agitation in 2-propanol, acetone, methanol, and deionized (DI) water. For the native oxide removal, Si substrates were further dipped into dilute hydrofluoric acid solution (HF, 2 vol%) for ~2 min, then rinsed with DI water and dried with N_2. The substrates were then immediately loaded to the reactor using a load lock and kept at the deposition temperature for at least 20 min before the process was initiated. All depositions were started with the metalorganic pulse. Trimethylaluminum ($AlMe_3$) and trimethylgallium ($GaMe_3$) were used as the Al and Ga precursors, respectively. $AlMe_3$ was kept at room temperature, whereas $GaMe_3$ was cooled down to 6 °C using a home-made Peltier cooling system. 5N-grade NH_3, N_2 and H_2 plasma gases, and the carrier gas, Ar, were further purified using MicroTorr gas purifiers. Metalorganic precursor pulses and plasma gases were carried from separate lines by 30 and 100 sccm Ar, respectively. The speed of the Adixen ATH 400 M turbo pump was adjusted in order to obtain a base pressure of ~150 mTorr. Remote plasma (300 W) was activated at each cycle only during the flow of N-containing plasma gas. Unless stated otherwise, the system was purged for 10 s after each exposure.

Film characterization

Ellipsometric spectra were recorded in the wavelength range of 300–1000 nm for AlN, and 400–1200 nm for GaN and $Al_xGa_{1-x}N$ thin films at three angles of incidence (65°, 70°, and 75°) using a variable angle spectroscopic ellipsometer (V-VASE, J.A. Woollam Co. Inc.) with a rotating analyzer. Optical constants and film thicknesses were extracted using the Cauchy dispersion function using a two-layer model; *i.e.* Cauchy/Si (0.5 mm). Chemical compositions and bonding states were determined by X-ray photoelectron spectroscopy (XPS) using a Thermo Scientific K-Alpha spectrometer with a monochromatized Al K_α X-ray source. The pass energy, step size, and spot size were 30 eV, 0.1 eV, and 400 μm, respectively. Etching of the samples was carried out *in situ* with a beam of Ar ions having an acceleration voltage of 1 kV. High-resolution XPS (HR-XPS) data were corrected for charging by shifting peaks with respect to the adventitious C peak located at 284.8 eV. Peak deconvolution was performed using the Avantage Software, without applying any restrictions to spectral location and full width at half maximum (FWHM) values. Secondary ion mass spectroscopy (SIMS) measurements were realized by the Evans Analytical Group (EAG) using a Physical Electronics Quadrupole SIMS instrument. Analyses were carried out using EAG's proprietary analytical protocols. Calibrations were based on relevant AlN, GaN and AlGaN internal standards for concentration and depth. Atomic mixing or depth resolution of the primary ion beam setup was <9 nm per decade. X-ray reflectivity (XRR) and grazing-incidence X-ray diffraction (GIXRD) measurements were carried out with a PANalytical X'Pert PRO MRD diffractometer using Cu K_α radiation. GIXRD patterns were obtained by performing 10 repeated scans within the 2theta range of 20–80° with a step size of 0.1° and a counting time of 10 s. These scans were then added together in order to obtain a single GIXRD pattern with good intensity values. Peak positions and the corresponding interplanar spacing values were obtained by fitting the GIXRD data using PANalytical X'Pert HighScore Plus Software. Using the same software, line profile analysis (LPA) was applied to each GIXRD pattern. Instrumental broadening was corrected using a polycrystalline silicon monitor sample, whose GIXRD data were obtained by performing 3 repeated scans within the 2theta range of 10–145° with a step size and a counting time of 0.06° and 10 s, respectively. XRR data were fitted by the PANalytical X'Pert Reflectivity Software using a four-layer model, *i.e.* Al_2O_3 (or Ga_2O_3)/AlN (or GaN)/SiO_2/Si. An FEI Tecnai G2 F30 transmission electron microscope (TEM) at an operating voltage of 300 kV was used for the imaging of samples prepared using an FEI Nova 600i Nanolab focused ion beam (FIB) system. The samples were prepared at an acceleration voltage of 30 kV, using various beam currents ranging from 50 pA to 21 nA. For the GaN and $Al_xGa_{1-x}N$ thin film samples, damage layers formed at the film/substrate interfaces were treated by FIB milling using beam voltages of 5 and 2 kV, respectively. An atomic force microscope (AFM, Park Systems Corp., XE-100) operating in the contact mode was used to reveal surface morphologies of the deposited thin films. Normal incidence transmission measurements were performed relative to air within the range of 220–900 nm using an Ocean Optics UV-VIS-NIR single beam spectrophotometer (HR4000CG-UV-NIR).

Results and discussion

AlN and GaN thin films deposited using non-optimized HCPA-ALD parameters

AlN and GaN thin films were first deposited on 4″ Si (100) substrates at 200 °C using non-optimized process parameters. 800 cycles were deposited, where one cycle consisted of: 0.1 s $AlMe_3$ or 0.015 s $GaMe_3$/10 s Ar purge/40 s, 300 W NH_3 plasma (50 sccm) or N_2/H_2 plasma (50 sccm each)/10 s Ar purge. Table 1 summarizes the spectroscopic ellipsometry (SE) results obtained from AlN and GaN thin film samples deposited using NH_3 and N_2/H_2 plasma processes, where the average thickness (t_{avg}), average refractive index (n_{avg}), and uniformity data were obtained by the evaluation of spectra taken from five different points on the Si 4″ wafer (the center and the edges). The growth per cycle (GPC) was calculated by dividing t_{avg} by the number of cycles applied, assuming that a constant amount of material was deposited in each cycle. When compared to N_2/H_2 plasma, the use of NH_3 plasma resulted in slightly higher GPC values for both AlN and GaN thin films. On the other hand, films deposited using N_2/H_2 plasma were better in terms of thickness uniformity. Although these deposition experiments were carried out using HCPA-ALD parameters that are not optimized for true ALD conditions, the resulting films were reasonably uniform with a wafer-level uniformity of $\leq \pm 1.5\%$. It is also worth mentioning that we achieved higher GPC values for AlN (1.02 and 0.96 Å for NH_3 and N_2/H_2 plasma processes, respectively) using the present configuration; GPC values that we obtained

Table 1 SE results of AlN and GaN thin films deposited using non-optimized HCPA-ALD parameters

Sample	t_{avg} (nm)	Uniformity[a] of t (±%)	GPC (Å)	n_{avg}[b]	Uniformity[a] of n (±%)
AlN (NH_3 plasma)	81.5	1.23	1.02	1.98	0.04
AlN (N_2/H_2 plasma)	76.7	1.05	0.96	1.99	0.15
GaN (NH_3 plasma)	21.1	1.51	0.26	2.17	0.50
GaN (N_2/H_2 plasma)	18.4	1.31	0.23	2.14	0.17

[a] Uniformity (±%) is calculated by the formula: [(max − min)/(2 × avg)] × 100. [b] n_{avg} is the average refractive index at 632 nm.

using the previous configuration with a quartz-based ICP source (described elsewhere[21]) were 0.86 (ref. 21) and 0.55 Å (ref. 23) for NH_3 and N_2/H_2 plasma processes, respectively. Although this improvement may be related to the higher plasma density of the HCP source, this cannot be stated for sure since the base pressure and Ar carrier flow rates were not the same for the current and previous configurations. Refractive indices of the AlN thin films deposited using NH_3 and N_2/H_2 plasma were 1.98 and 1.99 at 632 nm, respectively, which are higher than the values measured for AlN thin films deposited using the quartz-based ICP source and in good agreement with the values given in the literature for polycrystalline AlN thin films.[52] We measured the refractive indices of GaN films deposited using NH_3 and N_2/H_2 plasma to be 2.17 and 2.14, respectively, which are comparable to values given in the literature.[53]

XPS survey scans detected 6–11 at.% C and 15–30 at.% O on the AlN and GaN film surfaces. AlN surfaces were more prone to atmospheric oxidation (25–30 at.% O) as compared to GaN surfaces (15–16 at.% O). Additional XPS survey scans were obtained with constant time intervals (*e.g.* 60 s) as the samples in the ultra high vacuum (UHV) chamber of the XPS system were etched with a beam of Ar ions. For all the four samples, the C 1s peak disappeared with the first etch; therefore no C was detected in the subsequent scans. O concentrations in the AlN thin films gradually decreased with each etch, and became constant for $t_{etch} \geq 300$ s. The XPS survey scan obtained after 600 s of etch revealed the elemental composition of the AlN thin film deposited using NH_3 plasma to be 50.45 at.% Al, 45.56 at.% N, and 2.45 at.% O. The remaining 1.54 at.% corresponds to Ar, which incorporates into the samples during ion etching. The elemental composition of the AlN deposited using N_2/H_2 plasma was very similar to that deposited using NH_3 plasma. The survey scan ($t_{etch} = 600$ s) indicated 50.77 at.% Al, 44.90 at.% N, 2.97 at.% O, and 1.37 at.% Ar for this sample. These results indicate that the AlN films are slightly Al-rich with Al/N ratios of 1.11 and 1.13 for the samples deposited using NH_3 and N_2/H_2 plasma processes, respectively. Elemental compositions of the GaN thin films were also determined using XPS ($t_{etch} = 60$ s), where 42.19 at.% Ga, 55.18 at.% N, 1.51 at.% O, 1.13 at.% Ar, and 42.24 at.% Ga, 54.57 at.% N, 1.65 at.% O, and 1.54 at.% Ar were detected for the samples deposited using NH_3 and N_2/H_2 plasma, respectively. Although these results suggest N-rich GaN films, it should be noted that the atomic concentration of N is overestimated due to the significant contribution of Auger Ga peaks, which overlap with the N 1s peak.

In terms of O impurity concentrations determined by XPS, it seems that the use of the HCP source did not result in any improvement as we already reported <3 at.% O for AlN films deposited using the ICP source.[21,23] However it should be noted that the determination of impurity concentrations by XPS can be challenging. Butcher *et al.*[54] reported that using XPS to examine AlN thin films after etching the surface with a 5 kV argon ion beam results in substantial errors in the quantification of O and C impurities present in this material. In another study,[55] it was reported that XPS can detect 2–5 at.% O – again after Ar ion etching – for commercial GaN samples which have approximately 0.02% bulk O as confirmed by SIMS. In order to further investigate this, we obtained SIMS depth profiles for AlN and GaN thin films deposited using NH_3 plasma (Fig. 1). SIMS

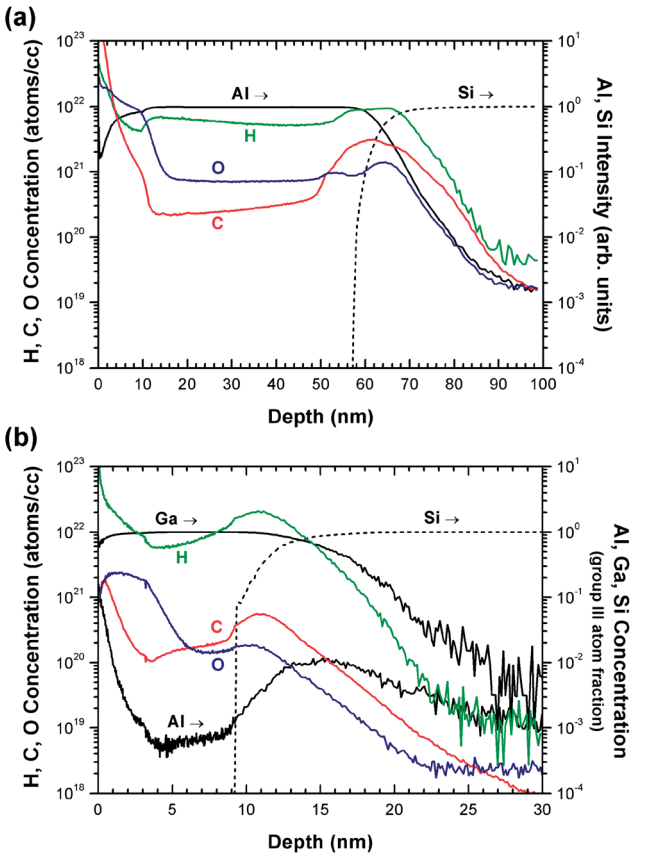

Fig. 1 Impurity concentrations determined by SIMS depth profiling for (a) AlN and (b) GaN thin films deposited using NH_3 plasma. Silicon is not quantified in the layers, only plotted as the substrate layer marker.

data showed that H, C, and O impurities present in both films. Concentrations of O and C were 6.9×10^{20} and 2.5×10^{20} atoms per cm^3 in the bulk AlN film (depth = 30 nm) (Fig. 1(a)), both of which correspond to <1 at.%. In the literature, similar quantities of O and C impurities were reported for AlN thin films deposited using PA-ALD.[29] The SIMS depth profile of the GaN film is given in Fig. 1(b), where the lower plateau (7–10 nm) reveals the real concentration of O in the GaN layer. The higher O concentration in the 0–5 nm region is an artifact from ion mixing from the surface O. Concentrations of O and C impurities were determined to be 1.4×10^{20} and 1.8×10^{20} atoms per cm^3 in the bulk GaN film (depth = 7 nm), both corresponding to <1 at.%. Concentrations of the H impurities were high in both films with values of 5.6×10^{21} and 8.0×10^{21} atoms per cm^3 for AlN and GaN, respectively. This observation is in parallel with the results recently published by Perros *et al.*,[27] which emphasize the presence of high concentrations (~20 at.%) of H impurities in AlN thin films deposited by PA-ALD using NH_3 and N_2/H_2 plasma. Film thicknesses estimated by SIMS were lower than those measured using SE, which is probably due to the different etch rates of AlN and GaN thin films deposited using HCPA-ALD and the standard samples used to quantify impurity concentrations.

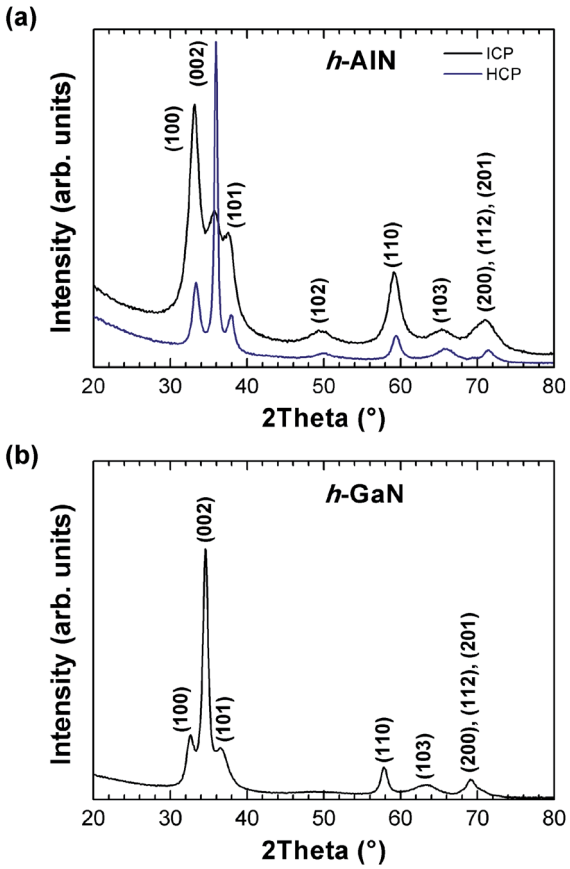

Fig. 2 GIXRD patterns of (a) AlN and (b) GaN thin films deposited on Si (100) substrates using NH_3 plasma. The GIXRD pattern of the AlN thin film deposited using a quartz-based ICP source[21] is also shown in (a) for comparison.

GIXRD patterns of AlN and GaN thin films deposited using NH_3 plasma are given in Fig. 2. The same GIXRD patterns were obtained for the AlN and GaN thin films deposited using N_2/H_2 plasma (not shown here); the use of different plasma gases (NH_3 *vs.* N_2/H_2 plasma) affected neither the peak positions nor the relative intensities of peaks. As revealed by their GIXRD patterns, AlN and GaN films were polycrystalline with (hexagonal) wurtzite crystal structure. Crystallite size values were calculated from the (002) reflections using LPA. Since the size-strain broadening was quite anisotropic we were not able to determine an average value using the Williamson–Hall plot. Crystallite sizes were found to be 19.2 and 24.8 nm for AlN, and 10.2 and 9.3 nm for GaN films deposited using NH_3 and N_2/H_2 plasma processes, respectively. The GIXRD pattern of the AlN thin film deposited using the quartz-based ICP source is also included in Fig. 2(a) for comparison. The increase in the intensity of the (002) reflection and improvement in the FWHM values suggest larger crystallites and therefore an enhancement in the crystalline quality for films deposited using the current configuration with the HCP source. LPA analysis results obtained for the (002) reflections showed that the crystallite sizes, which were 3.4 and 3.1 nm for AlN films deposited using NH_3 and N_2/H_2 plasma, respectively, increased to 20–25 nm with the use of the present configuration. Assuming that a significant fraction of O impurities segregate at the grain boundaries, the increase in crystallite size might indicate a decrease in the O impurity concentration. Fig. 3(a) and (b) show the TEM and high-resolution TEM (HR-TEM) images of the GaN thin film deposited using NH_3 plasma. The ~3 nm thick amorphous SiO_2 layer at the GaN/Si interface, which is generally named as the "damage layer", formed during the TEM sample preparation using FIB.[56] The thickness of the GaN layer was measured from the HR-TEM image (Fig. 3(b)) to be 19.2 nm, which is ~2 nm lower than the value measured using SE (*i.e.* 21.1 nm). XRR, on the other hand, yielded a thickness of 18.2 nm for this sample (sum of the GaN and Ga_2O_3 layer thicknesses in the 4-layer XRR model), which is slightly lower than the value directly measured from the HR-TEM image. Besides confirming the polycrystallinity of the GaN layer, the HR-TEM image also evidences the existence of large crystals in the film, which can extend along the film thickness. Diffraction rings seen in the SAED pattern (Fig. 3(c)) also reveal the polycrystalline nature of the GaN thin film, whereas reciprocal lattice points in this pattern correspond to the diamond lattice of the underlying Si (100) substrate.

Optimization of HCPA-ALD parameters

AlN thin films. HCPA-ALD parameters were optimized at 200 °C for the deposition of AlN thin films using $AlMe_3$ and N_2/H_2 plasma. For the $AlMe_3$ saturation curve (Fig. 4(a)) 200 cycles AlN were deposited on Si (100) substrates using different $AlMe_3$ pulse lengths, where one HCPA-ALD cycle was 0.03–0.12 s $AlMe_3$/10 s Ar purge/40 s, 50 + 50 sccm, 300 W N_2/H_2 plasma/10 s Ar purge. As seen in Fig. 4(a), the GPC values calculated using SE and XRR data followed the same trend with different values, and the GPC slightly decreased with increasing $AlMe_3$

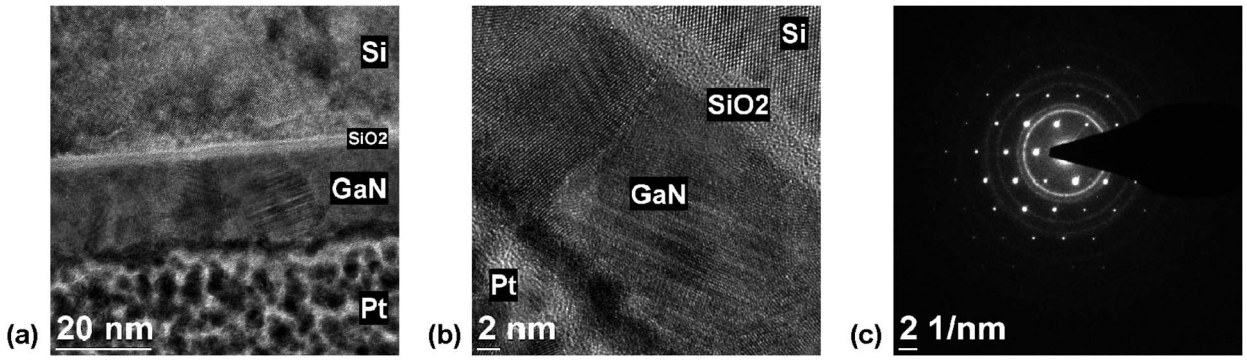

Fig. 3 Cross-sectional (a) TEM and (b) HR-TEM images of a 21 nm thick GaN thin film deposited on a Si (100) substrate using NH_3 plasma. The FIB-induced SiO_2 damage layer formed at the GaN/Si interface during TEM sample preparation. (c) SAED pattern of the same sample.

pulse lengths. Physically, such a decrease is not possible since as the pulse length increases the amount (or number) of $AlMe_3$ molecules that are being carried to the reactor increases, which in turn increases the number of collisions the reactant has with the surface. Precursors may desorb from the surface when long purge times are used, however this should not be the case here since a constant purge time of 10 s was used for all depositions. Therefore the slight decrease in GPC was considered to be within the limits of measurement error, and ignored, and GPC was accepted as a constant at ~0.93 Å (as measured by SE) for the $AlMe_3$ pulse length range of 0.03–0.12 s. Although 0.03 s $AlMe_3$ seems to be enough for having self-limiting surface reactions, we selected 0.06 s as the optimized value for the following depositions. As the next step of optimization study, the flow duration of N_2/H_2 plasma was varied while keeping the other parameters constant (Fig. 4(b)). The data obtained using SE and XRR revealed different trends. According to the curve plotted using XRR data, the GPC first slightly increases and then reaches saturation for flow durations ≥40 s. According to the SE data, it increases from 0.89 to 0.99 Å with longer durations of N_2/H_2 flow within the 20–80 s range. It should be noted that since Si substrates were treated with HF prior to each deposition, the ellipsometric spectra were fitted using a two-layer model (*i.e.* Cauchy/Si (0.5 mm)) by assuming that the thickness of the SiO_2 layer at the AlN/Si interface was negligible. XRR data, on the other hand, were fitted using a four-layer model (*i.e.* $Al_2O_3/AlN/SiO_2/Si$); thicknesses of AlN and surface oxide (Al_2O_3) layers were added together for revealing the film thickness, which was then used for the calculation of the GPC value. When the thicknesses of native SiO_2 layers were also included to the film thickness values (shown in Fig. 4(b)), the results resembled those obtained by SE, where no saturation behavior was observed. Although the applicability of the Cauchy dispersion function for the determination of the AlN film thickness was verified by TEM,[21] the results suggest that the increase in GPC values obtained by SE for N_2/H_2 flow durations ≥40 s is due to the contribution of the native oxide layer. Therefore, it can be presumed that the self-limiting surface reactions are achieved for AlN deposition when 40 s or longer N_2/H_2 plasma is used with predetermined N_2 and H_2 flow rates. Another parameter, which needs to be optimized, is the purge time. If the purge time is not long enough, then the precursor might be introduced into the chamber before the other one is completely purged away. This would result in gas-phase reactions and a significant CVD component in the deposited films. In order to optimize this parameter for the deposition of AlN thin films, we did additional depositions using 5 and 20 s purge time, where the $AlMe_3$ pulse length was 0.06 s and the N_2/H_2 flow duration was 40 s. The GPC values, which were calculated using SE results, were found to be

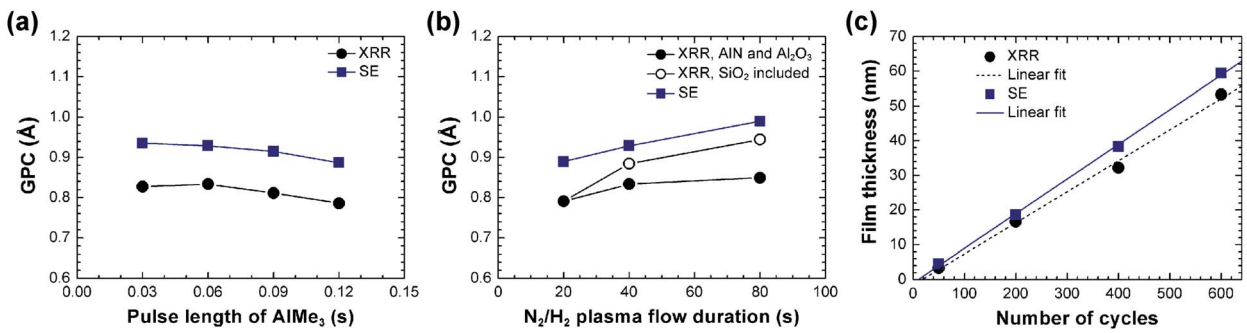

Fig. 4 (a) $AlMe_3$ and (b) N_2/H_2 saturation curves at 200 °C. For the $AlMe_3$ saturation curve, the N_2/H_2 flow rate and flow duration were kept constant at 50 + 50 sccm and 40 s, respectively. The $AlMe_3$ pulse length was 0.06 s for the N_2/H_2 saturation curve. (c) The AlN film thickness plotted as a function of the number of deposition cycles.

0.90, 0.93, and 0.92 Å for 5, 10, and 20 s of purging, respectively. This confirms that 10 s purging is long enough to avoid any gas-phase reactions, and even 5 s can be used to have shorter cycles. The optimized recipe was therefore determined for the AlN growth to be 0.06 s $AlMe_3$/10 s Ar purge/40 s, 50 + 50 sccm, 300 W N_2/H_2 plasma/10 s Ar purge. In Fig. 4(c), the AlN film thicknesses measured using SE and XRR were plotted as a function of the number of cycles. Results indicated linear growth with a slight nucleation delay. The slope of the linear fit of SE data revealed the GPC at 200 °C to be ~1.0 Å.

GaN thin films. HCPA-ALD parameters were optimized at 200 °C for the deposition of GaN thin films using $GaMe_3$ and N_2/H_2 plasma, where 300 cycles were deposited using 0.015–0.09 s $GaMe_3$/5–20 s Ar purge/20–80 s, 50 + 50 s, 300 W N_2/H_2 plasma/5–20 s Ar purge. Fig. 5(a) shows the $GaMe_3$ saturation curve, which was obtained by varying the $GaMe_3$ pulse length between 0.015 and 0.09 s, while keeping the purge time and N_2/H_2 plasma flow duration constant at 10 and 40 s, respectively. SE and XRR data revealed curves with similar shapes but slightly different values. When the $GaMe_3$ pulse length was increased from 0.015 to 0.03 s, the GPC (determined by SE) negligibly increased from 0.30 to 0.31 Å; for 0.06 and 0.09 s it was 0.32 Å. Therefore, the GPC was constant within the range of 0.015–0.09 s, which evidences the self-limiting growth of GaN. In the following step, the N_2/H_2 plasma duration was varied between 20 and 80 s (Fig. 5(b)). The $GaMe_3$ pulse length and purge time were 0.03 and 10 s, respectively. According to both SE and XRR data, the GPC increased upon increasing the N_2/H_2 flow duration from 20 to 40 s, but then saturated and did not change when the flow duration was further increased to 80 s, which again clearly indicates the existence of a "self-limiting" growth mechanism. Therefore, optimized values of the $GaMe_3$ pulse length and N_2/H_2 flow duration were determined to be 0.03 and 40 s, respectively. The effect of the purge time was studied by performing depositions with purge times of 5, 10, and 20 s, all of which resulted with the same GPC. Therefore the optimized recipe for GaN deposition was determined to be 0.03 s $GaMe_3$/10 s Ar purge/40 s, 50 + 50 sccm, 300 W N_2/H_2 plasma/10 s Ar purge. Fig. 5(c) shows GPC values for the optimized recipe, which were plotted as a function of the number of cycles. Both SE and XRR data show a similar trend, where the GPC decreases with an increasing number of deposition cycles. This suggests substrate-enhanced growth, where the GPC of GaN on Si is higher when compared to that of GaN on itself. This kind of growth behavior can occur if the number of reactive sites on the substrate is higher than on the ALD-grown material.[6]

AlN and GaN thin films deposited using optimized HCPA-ALD parameters

600 cycles AlN and 900 cycles GaN were deposited at 200 °C using optimized HCPA-ALD parameters. Table 2 summarizes the SE results of these thin film samples together with the results of AlN and GaN films deposited using N_2/H_2 plasma with non-optimized parameters. Note that the non-optimized parameters used for the deposition of AlN and GaN thin films using N_2/H_2 plasma were identical to the optimized parameters except the pulse lengths of $AlMe_3$ and $GaMe_3$. Furthermore, it has been shown in the previous section that the metalorganic pulse lengths used in the non-optimized recipes (0.1 s for $AlMe_3$ and 0.015 s $GaMe_3$) also result in a self-limiting growth mechanism (see Fig. 4(a) and 5(a)). For both AlN and GaN thin films, the use of optimized HCPA-ALD parameters resulted in a better thickness uniformity over a 4″ Si substrate. Refractive indices of AlN (0.06 s $AlMe_3$) and GaN (0.015 s $GaMe_3$) thin films were found to be 1.94 and 2.14 at 632 nm, respectively. These values increased to 1.99 and 2.17 when higher metalorganic pulse lengths were employed, which might be due to the deposition of denser films. Refractive index values of AlN and GaN films determined by the Cauchy dispersion function are both in good agreement with those reported in the literature.[52,53]

The change in metalorganic pulse lengths did not affect the chemical compositions of films. Chemical bonding states at the film surface ($t_{etch} = 0$ s) and in the bulk film ($t_{etch} = 300$ and 60 s for AlN and GaN, respectively) were determined for the samples deposited using optimized parameters by the evaluation of their HR-XPS scans (Fig. 6 and 7). The Al 2p HR-XPS scan obtained from the AlN film surface (Fig. 6(a)) was fitted by two subpeaks (subpeaks A and B) located at 73.78 and 72.92 eV, corresponding to Al–O[57] and Al–N[57,58] bonds, respectively. Upon Ar ion etching, subpeak A (corresponding to the Al–O bond) disappeared, and therefore the Al 2p HR-XPS scan was fitted with a single peak

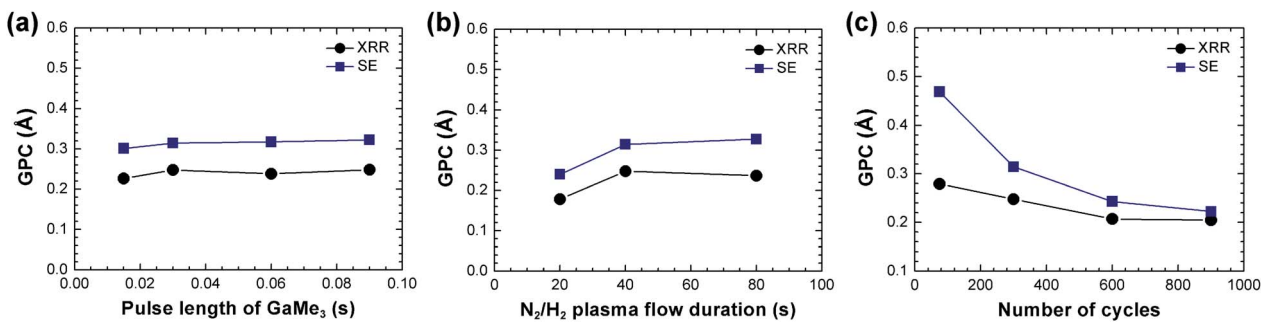

Fig. 5 (a) $GaMe_3$ and (b) N_2/H_2 saturation curves at 200 °C. For the $GaMe_3$ saturation curve, the N_2/H_2 flow rate and flow duration were kept constant at 50 + 50 sccm and 40 s, respectively. The $GaMe_3$ pulse length was 0.03 s for the N_2/H_2 saturation curve. (c) The GPC plotted as a function of the number of deposition cycles. Data suggest substrate-enhanced growth of GaN thin films.

Table 2 SE results of AlN and GaN thin films deposited using N_2/H_2 plasma

Sample	t_{avg} (nm)	Uniformity[b] of t (±%)	GPC (Å)	n_{avg}[c]	Uniformity[b] of n (±%)
AlN (0.06 s $AlMe_3$)[a]	59.2	0.57	0.99	1.94	0.28
AlN (0.1 s $AlMe_3$)	76.7	1.05	0.96	1.99	0.15
GaN (0.015 s $GaMe_3$)	18.4	1.31	0.23	2.14	0.17
GaN (0.03 s $GaMe_3$)[a]	20.1	0.77	0.22	2.17	0.32

[a] Optimized values for the HCPA-ALD of AlN and GaN thin films. [b] Uniformity (±%) is calculated by the formula: [(max − min)/(2 × avg)] × 100. [c] n_{avg} is the average refractive index at 632 nm.

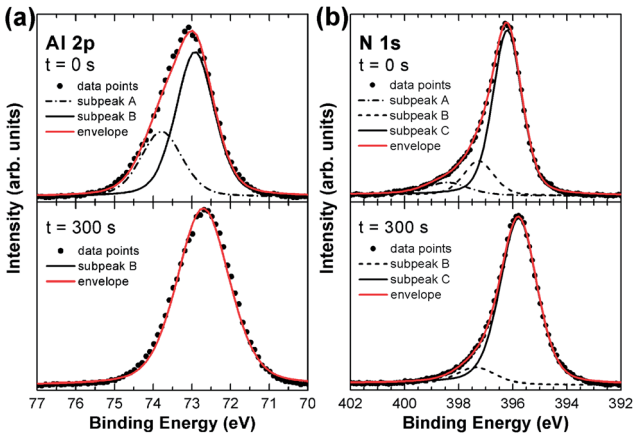

Fig. 6 (a) Al 2p and (b) N 1s HR-XPS scans of a 59.2 nm thick AlN thin film deposited on a Si (100) substrate using optimized HCPA-ALD parameters.

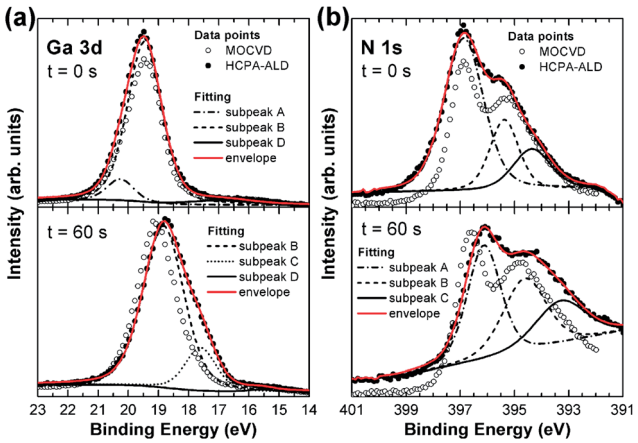

Fig. 7 (a) Ga 3d and (b) N 1 s HR-XPS scans of a 20.1 nm thick GaN thin film deposited on a Si (100) substrate using optimized HCPA-ALD parameters.

(subpeak B, 72.71 eV), which was attributed to the Al–N bonding state. Additional information about the chemical bonding states in the AlN film was provided by the N 1s spectrum (Fig. 6(b)). The N 1s scan obtained from the AlN film surface was fitted using three subpeaks located at 398.42 (subpeak A), 397.27 (subpeak B), and 396.20 eV (subpeak C), corresponding to N–Al–O (surface only),[58] N–Al–O,[58] and N–Al[58,59] bonds, respectively. The N 1s HR-XPS scan obtained after Ar ion etching revealed the existence of N–Al–O (subpeak B, 397.37 eV) and N–Al (subpeak C, 395.79 eV) bonds in the bulk film. Subpeaks corresponding to Al–N and N–Al bonds in the Al 2p and N 1s spectra, respectively, confirmed the presence of AlN, whereas the oxynitride peak (N–Al–O) was related to the <3 at.% O in the bulk film detected by the XPS survey scan.

Ga 3d and N 1s HR-XPS spectra of the GaN thin film sample are shown in Fig. 7(a) and (b), respectively. Ga 3d and N 1s spectra obtained from a commercial MOCVD-grown GaN sample were also included in these figures for comparison. The Ga 3d scan revealed the existence of Ga–O[60,61] and Ga–N[60–62] bonds at the film surface with subpeaks A (20.27 eV) and B (19.46 eV), respectively. Subpeak D located at 16.98 eV was related to the contribution from the N 2s core level.[61,63] The N 1s spectrum obtained from the film surface was fitted using three subpeaks located at 396.87 (subpeak A), 395.37 (subpeak B), and 394.36 eV (subpeak C). Subpeak A was assigned to the N–Ga bond,[64] whereas subpeaks B and C were identified as the Auger Ga peaks.[65] Ga 3d and N 1s spectra obtained from the surface of the GaN thin film deposited by HCPA-ALD were in good agreement with those obtained from the surface of the commercial MOCVD-grown sample. The Ga 3d HR-XPS spectrum of the etched film was fitted with three subpeaks located at 18.83 (subpeak B), 17.60 (subpeak C), and 15.61 eV (subpeak D), corresponding to Ga–N and Ga–Ga[62] bonding states, and contribution from the N 2s core level, respectively. It is believed that the Ga–Ga bond is not associated with the sample, but forms during Ar ion etching due to the accumulation of metallic Ga on the surface of the GaN thin film sample.[55,66] The N 1s spectrum obtained from the etched film was fitted using three subpeaks, which were again assigned to the N–Ga bond (subpeak A, 396.23 eV) and Auger Ga peaks (subpeak B, 394.72 eV and subpeak C, 393.39 eV). The spectral locations of the subpeaks corresponding to a particular bonding state, contribution, or Auger peak shifted to lower binding energies for etched GaN samples. The spectral locations of Ga 3d and N 1s peaks (t_{etch} = 60 s) were also found to be slightly different for HCPA-ALD- and MOCVD-grown GaN samples. This might be related to the reference that we used for the correction of charging effects. For etched samples it is generally convenient to use the spectral position of the Ar 2p peak for determining the amount of shift needed. However, in our case, Ar 2p peaks were quite weak to be used for correction. Therefore we shifted the HR-XPS spectra of etched samples – as we were shifting the spectra obtained from the film surface – by an amount determined by the location of the adventitious C peak (C 1s). This approach might not work,

as in the present case, if charging of the film surface and the etched region are different due to their distinct chemical compositions.

GIXRD patterns of the AlN and GaN thin films deposited on Si (100) and Si (111) substrates using optimized HCPA-ALD parameters (shown in part in Fig. 10 and 11) were identical to those given in Fig. 2(a) and (b), respectively, in terms of peak positions and relative intensities of the peaks. As their GIXRD indicated, AlN and GaN thin films deposited at 200 °C were single-phase and polycrystalline with hexagonal wurtzite crystal structure. The GIXRD pattern of the 59.2 nm thick AlN thin film deposited on a *c*-plane sapphire substrate was slightly different than those obtained from samples deposited on Si (100) and Si (111) substrates. The same seven reflections of the *h*-AlN phase appeared at exactly the same 2theta positions, however the intensity of the (100) reflection was almost as high as that of the (002) reflection. The intensity of the (103) reflection was also slightly higher for the sample deposited on *c*-plane sapphire substrates. In the case of GaN, the difference between GIXRD patterns of thin films deposited on Si and *c*-plane sapphire substrates was remarkable. Fig. 8 shows the GIXRD pattern of a 20.1 nm thick GaN thin film deposited on *c*-plane sapphire substrate. (101) and (110) reflections and the peak that encloses (200), (112), and (201) reflections disappeared for this sample. The intensities of (100) and (002) reflections decreased, and the intensity of (103) reflection increased significantly. It should be noted that the GIXRD method, because of its geometry, is insensitive to the planes that are parallel to the substrate, therefore the disappearance of the peaks might be an indication of preferred orientation.

XRR results of AlN and GaN thin films deposited on Si (100) substrates using N_2/H_2 plasma with optimized HCPA-ALD parameters are given in Table 3. Film thicknesses estimated by XRR were lower than those measured using SE. As shown previously, the actual film thickness lies between the values measured by SE and XRR. The mass densities (ρ) of AlN and GaN thin films were estimated to be 2.82 and 5.86 g cm^{-3}, which are lower than the recognized values of 3.23 and 6.15 g cm^{-3}, respectively.[67] The estimated mass density of the AlN thin film (2.82 g cm^{-3}) was higher than those reported in the literature for AlN films deposited by PA-ALD at 200 °C (ρ = 2.34–2.65 g cm^{-3}).[24,27] XRR also revealed the rms roughnesses of these AlN and GaN thin films to be 2.16 and 1.54 nm, which are higher than the values directly measured using AFM. Fig. 9 shows the 2D surface morphologies of AlN and GaN thin films deposited on Si (100) substrates. Rms roughnesses of the AlN and GaN thin films were measured from a 1 μm × 1 μm scan area to be 1.97 and 0.64 nm, respectively. Rms surface roughnesses were 1.96 and 0.51 nm for AlN and GaN thin films deposited on Si (111) substrates, and 1.62 and 0.26 nm for AlN and GaN thin films deposited on *c*-plane sapphire substrates.

Table 3 XRR results of AlN and GaN thin films deposited using optimized HCPA-ALD parameters

Sample	$t_{Nit.}$[a] (nm)	$t_{Ox.}$[b] (nm)	ρ (g cm^{-3})	r_{rms} (nm)
AlN	53.21	0.09	2.82	2.16
GaN	17.00	1.40	5.86	1.54

[a] $t_{Nit.}$ is the thickness of the nitride layer; *i.e.* AlN or GaN. [b] $t_{Ox.}$ is the thickness of the surface oxide layer; *i.e.* Al_2O_3 or Ga_2O_3.

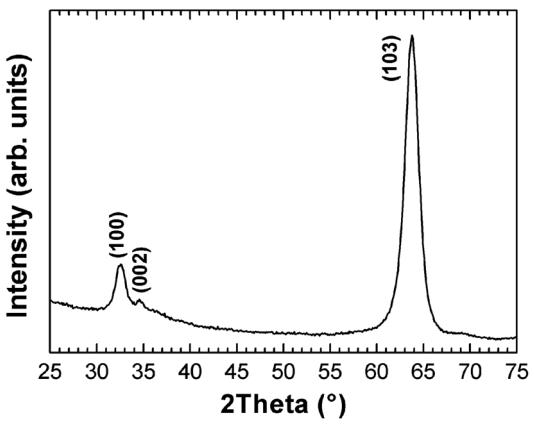

Fig. 8 GIXRD pattern of a 20.1 nm thick GaN thin film deposited on a *c*-plane sapphire substrate using optimized HCPA-ALD parameters.

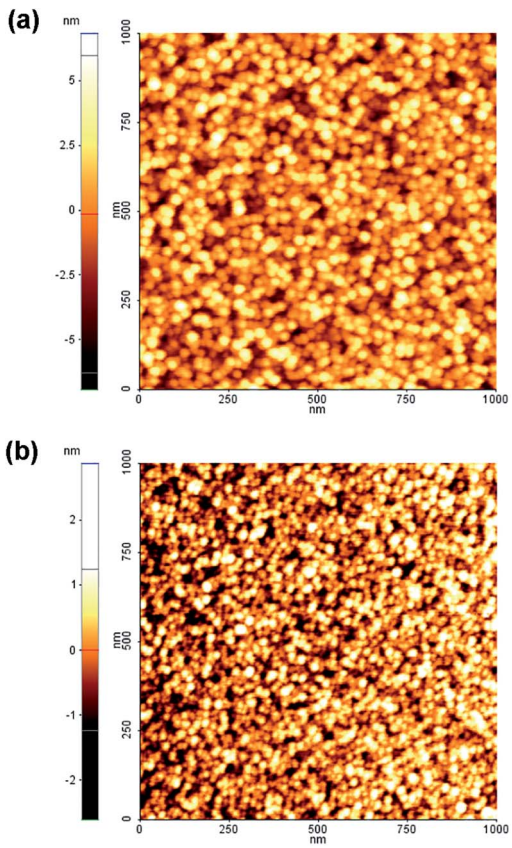

Fig. 9 Surface morphologies of (a) 59.2 nm thick AlN and (b) 20.1 nm thick GaN thin films deposited on Si (100) substrates using optimized HCPA-ALD parameters.

AlN and GaN thin films deposited using N_2 plasma

The effect of the plasma gas composition on the properties of deposited nitride thin films was studied. For this purpose, AlN and GaN films were deposited on Si (100) substrates using N_2 plasma, as well as N_2/H_2 plasma with decreased H_2 flow (*i.e.* 25 sccm). SE results of these thin film samples are summarized in Table 4, where the thicknesses and refractive indices of the thin films deposited using N_2/H_2 plasma (50 + 25 sccm) were comparable to those of the films deposited using optimized parameters. Thicknesses of the AlN and GaN thin films increased tremendously when N_2 was used as the plasma gas. Furthermore, refractive index values decreased upon the use of N_2 plasma, which indicates deterioration of the film quality. GIXRD patterns of the AlN and GaN thin films deposited with N_2/H_2 and N_2 plasma are shown in Fig. 10(a) and (b), respectively, together with the GIXRD patterns of films deposited using the optimized HCPA-ALD parameters. As seen from these figures, decreasing the H_2 flow rate from 50 to 25 sccm did not affect the crystalline qualities of AlN and GaN thin films, the same GIXRD patterns were obtained in both cases. The use of N_2 plasma without any H_2, on the other hand, resulted in amorphous GaN thin films. In the case of AlN, the crystallinity is almost lost as the reflections of the hexagonal wurtzite phase became barely visible. We observed similar results for the AlN and GaN films deposited using the previous configuration with a quartz-based ICP source,[49] where the use of N_2 plasma resulted in high concentrations of C and O impurities in the deposited films and destroyed crystallinity. The presence of C impurities (8.0 and 9.1 at.% for AlN and GaN, respectively)[49] suggests that the organic ligands are trapped inside the growing film since N_2 plasma without any H_2 is not efficient in terms of removing the ligands of the chemisorbed trimethylmetal precursors. This might be avoided at higher temperatures, where the methyl ligands of the precursor molecules get free by self-decomposition. Although it has been thought that the high O concentrations in the films (48.5 and 4.5 at.% for AlN and GaN, respectively)[49] are related to plasma-related oxygen contamination, recently Perros *et al.*[27] showed that the N_2 plasma process results in unstable AlN films, which oxidize upon exposure to the atmosphere. It is also worth mentioning that there were particles on the surfaces of AlN and GaN films deposited using N_2 plasma. The particles were larger in the case of GaN thin film, which also showed color variations that indicate thickness non-uniformity. The formation of these particles cannot be attributed to gas-phase reactions since we have already shown that 10 s purging is sufficient to avoid overlapping of the trimethylmetal precursor and plasma gas (50 sccm N_2 together with 50 sccm H_2). Therefore, the only explanation would be the formation of solid byproducts as a result of the reaction between trimethylmetal compounds and N radicals. These results show that the N_2 plasma process is not eligible for the low-temperature deposition of AlN and GaN thin films.

Table 4 SE results of AlN and GaN thin films deposited using N_2/H_2[a] and N_2 plasma

Reactant	t_{AlN} (nm)	n_{AlN}	t_{GaN} (nm)	n_{GaN}
N_2/H_2 plasma[a]	57.2	1.94	20.6	2.18
N_2 plasma	83.6	1.59	111.1	1.88

[a] Flow rates of N_2 and H_2 were 50 and 25 sccm, respectively.

$Al_xGa_{1-x}N$ thin films deposited by digital alloying

$Al_xGa_{1-x}N$ thin films with different compositions were deposited at 200 °C on Si (100), Si (111), and *c*-plane sapphire substrates. In order to adjust the alloy composition, different numbers of AlN and GaN subcycles were used in the main cycle; *i.e.* AlN : GaN = 1 : 3, 1 : 1, and 3 : 1. 800 subcycles were

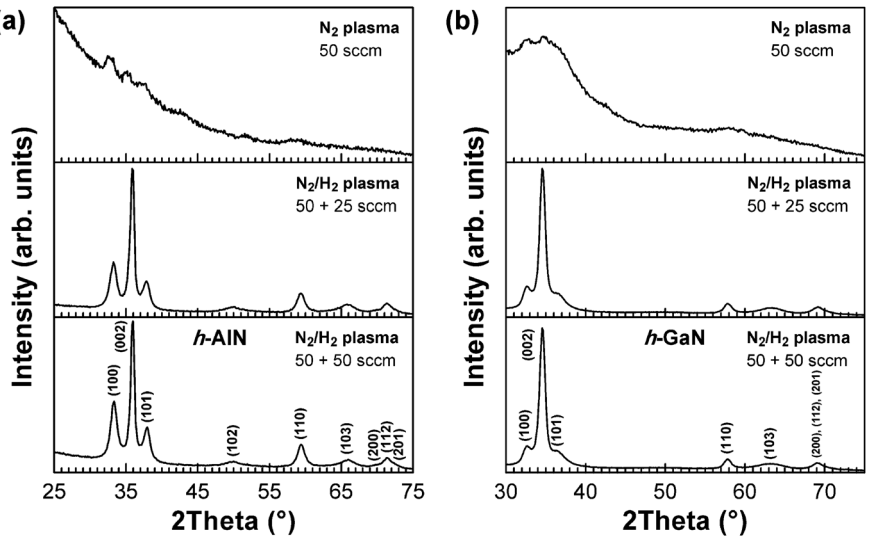

Fig. 10 GIXRD patterns of (a) AlN and (b) GaN thin films deposited on Si (100) substrates using N_2/H_2 (50 + 50 sccm), N_2/H_2 (50 + 25 sccm), and N_2 (50 sccm) plasma.

deposited in each case, where AlN subcycles were deposited using the optimized HCPA-ALD parameters, whereas GaN subcycles were deposited using the optimized recipe with 0.015 s $GaMe_3$ pulse length. GIXRD patterns of the $Al_xGa_{1-x}N$ thin films are shown in Fig. 11, together with those of AlN and GaN thin films deposited using optimized process parameters. As seen from these patterns, as the number of AlN subcycles increases, the peaks shift towards higher 2theta values due to the incorporation of Al into the wurtzite lattice. Using these data, the alloy composition, x, can be determined for each $Al_xGa_{1-x}N$ thin film using Vegard's rule, which simply states that the lattice parameters of an alloy will vary linearly between the end members.[68] It should be noted that this rule applies to unstrained materials, where composition is the only factor affecting the lattice parameters. For the c lattice parameter of $Al_xGa_{1-x}N$, Vegard's rule is given as:

$$c_{Al_xGa_{1-x}N} = xc_{AlN} + (1 - x)c_{GaN} \quad (1)$$

The interplanar spacing values calculated from peak positions using the well-known Bragg's law are annotated on Fig. 11 for (002) and (110) planes. Lattice parameters a and c were roughly calculated by substituting these d_{110} and d_{002} values, respectively, in the following formula (eqn (2)), which relates the interplanar spacing (d_{hkl}), miller indices (hkl) and lattice parameters (a and c) for hexagonal crystals. Alloy compositions, x, were then calculated from c lattice parameters using Vegard's rule (eqn (1)).

$$\frac{1}{d^2} = \frac{4}{3}\left(\frac{h^2 + hk + k^2}{a^2}\right) + \frac{l^2}{c^2} \quad (2)$$

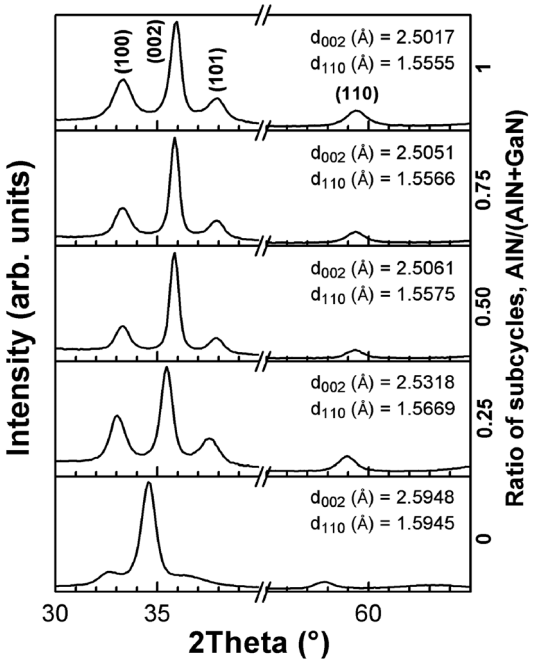

Fig. 11 GIXRD patterns of AlN, GaN, and $Al_xGa_{1-x}N$ thin films deposited on Si (100) substrates.

Theoretical values of alloy composition ($x_{Theo.}$) were also determined using the formula,

$$x_{Theo.} = \frac{n_{s\ AlN}GPC_{AlN}}{n_{s\ AlN}GPC_{AlN} + n_{s\ GaN}GPC_{GaN}} \quad (3)$$

where $n_{s\ AlN}$ is the number of AlN subcycles, $n_{s\ GaN}$ is the number of GaN subcycles, and GPC_{AlN} and GPC_{GaN} are the deposition rates of AlN and GaN (0.015 s $GaMe_3$) thin films, which were reported to be 0.99 and 0.23 Å per cycle, respectively, in the previous sections. The calculated lattice parameters, c/a ratios, and alloy compositions are summarized in Table 5.

Although the calculated a lattice parameters of AlN and GaN are in good agreement with those reported in the literature for their nominally strain-free counterparts, c lattice parameters were found to be higher (0.45% for AlN and 0.06% for GaN with respect to the highest c value reported in the literature) than those of strain-free AlN and GaN thin films.[68] These results indicate the presence of strain, which limit the applicability of Vegard's rule to $Al_xGa_{1-x}N$ thin films deposited by HCPA-ALD. In order to minimize errors, alloy compositions were calculated by substituting c lattice parameters of HCPA-ALD-grown AlN and GaN films into eqn (1). Theoretical values calculated using eqn (3) were lower than those found by Vegard's rule. However, it should be noted that the theoretical calculation of alloy composition is not straightforward in the present case since the deposition rate of AlN on GaN and/or the deposition rate of GaN on AlN might be different than those of AlN on AlN and GaN on GaN, respectively. Moreover, the HCPA-ALD of AlN exhibits a slight nucleation delay, and the GPC of GaN is higher in the beginning of growth (see Fig. 4(c) and 5(c)).

Thicknesses of the $Al_{0.68}Ga_{0.32}N$, $Al_{0.95}Ga_{0.05}N$ and $Al_{0.96}Ga_{0.04}N$ films were determined to be 25.4, 42.4, and 57.9 nm, respectively, using SE. These values were found to be lower than those calculated theoretically due to uncertainties in GPC values as discussed in the above paragraph. Cross-sectional bright-field scanning TEM (STEM) and HR-TEM images of the $Al_{0.68}Ga_{0.32}N$ thin film are shown in Fig. 12(a) and (b), respectively. From Fig. 12(a), it is seen that the $Al_{0.68}Ga_{0.32}N$ layer is highly uniform. The thickness of the $Al_{0.68}Ga_{0.32}N$ thin film was measured directly from Fig. 12(b) to be 26.3 nm, which is in good agreement with the result obtained from SE. The HR-

Table 5 Lattice parameters, c/a ratios, and alloy compositions of AlN, GaN, and $Al_xGa_{1-x}N$ thin films

RS[a]	c[b] (Å)	a[c] (Å)	c/a	$x_{Veg.}$[d]	$x_{Theo.}$[e]
0 (GaN)	5.1896	3.1889	1.627	0	0
0.25	5.0636	3.1338	1.616	0.68	0.59
0.50	5.0122	3.1151	1.609	0.95	0.81
0.75	5.0101	3.1133	1.609	0.96	0.93
1 (AlN)	5.0034	3.1110	1.608	1	1

[a] RS is the ratio of subcycles; *i.e.* $n_{s\ AlN}/(n_{s\ AlN} + n_{s\ GaN})$. [b] Calculated using the position of (002) reflection. [c] Calculated using the position of (110) reflection. [d] $x_{Veg.}$ is the alloy composition calculated from c values using Vegard's rule (eqn (1)). [e] $x_{Theo.}$ is the alloy composition calculated theoretically using GPC values (eqn (3)).

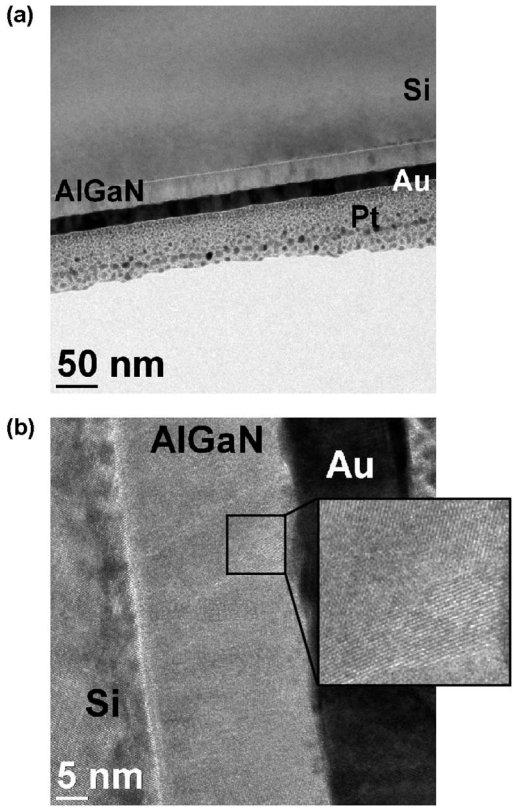

Fig. 12 Cross-sectional (a) bright-field STEM and (b) HR-TEM images of 25.4 nm thick $Al_{0.68}Ga_{0.32}N$ thin film deposited on a Si (111) substrate using N_2/H_2 plasma.

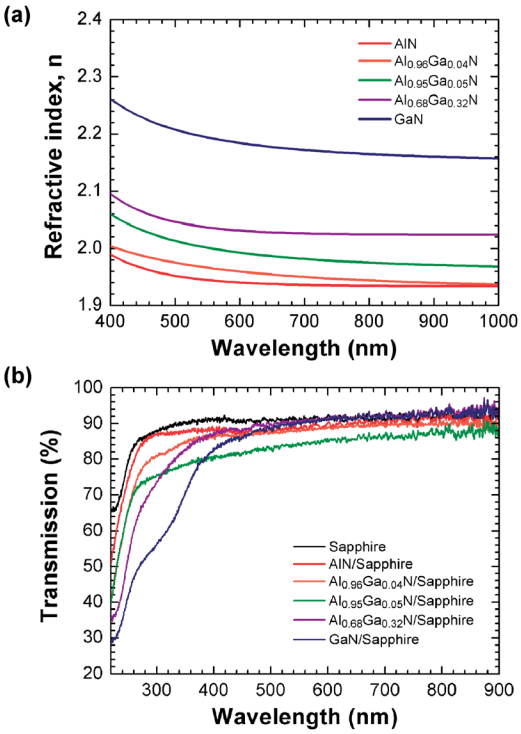

Fig. 13 (a) Spectral refractive indices and (b) optical transmission spectra of AlN, GaN, and $Al_xGa_{1-x}N$ thin films deposited on Si (100) and double side polished *c*-plane sapphire substrates, respectively.

TEM image (Fig. 12(b)) and SAED pattern (not shown here) revealed the polycrystalline nature of this sample, which has also been indicated in Fig. 11 for the film deposited on the Si (100) substrate.

In the previous sections, we reported the refractive index values of AlN (0.06 s $AlMe_3$) and GaN (0.015 s $GaMe_3$) to be 1.94 and 2.14 at 632 nm, respectively. Refractive index values decreased from 2.03 to 1.96 as the Al content of $Al_xGa_{1-x}N$ increased from 0.68 to 0.96 (Fig. 13(a)). Refractive indices of the $Al_xGa_{1-x}N$ thin films were found to be quite close to that of AlN ($n = 1.94$) since the ternary alloys deposited in this study were all Al-rich. Optical transmission spectra of AlN, GaN, and $Al_xGa_{1-x}N$ thin films deposited on double side polished sapphire substrates at 200 °C are shown in Fig. 13(b). The optical transmission spectrum of sapphire is also included in the figure. Film transmissions were found to be equal to the substrate transmission (~93%) in the visible spectrum, indicating absorption-free films. A significant decrease in the UV transmission was observed at wavelengths <260 nm, which is caused by the main band gap absorption. In addition, optical band edge values of the films shifted to lower wavelengths with increasing Al content. The transmission data obtained from a 20.1 nm thick GaN film exhibited a weak shoulder at lower wavelength values. The widening of the absorption edge particularly observed for this thin film sample might be attributed to strain-induced defects[69] and/or the quantum confinement effect[70] due to the small crystallite size, which was estimated to be 9.3 nm by the LPA.

Summary and conclusions

In this paper we have demonstrated the HCPA-ALD of crystalline AlN, GaN and $Al_xGa_{1-x}N$ thin films at low temperature (*i.e.* 200 °C) using trimethylmetal precursors and NH_3 or N_2/H_2 plasma. Preliminary depositions carried out using non-optimized process parameters resulted in reasonably uniform AlN and GaN films with wafer-level non-uniformities less than ±1.5%. XPS survey scans detected 2.5–3.0 and 1.5–1.7 at.% O in these AlN and GaN thin films, respectively, after they were etched *in situ* with a beam of Ar ions under UHV conditions. C was detected only at the film surfaces and there were no C impurities in the bulk films as determined by XPS. Since the Ar ion etching may lead to substantial errors in the quantification of O and C impurities present in AlN and GaN thin films, complementary SIMS analyses were performed on the films deposited using NH_3 plasma, which revealed the presence of O, C (both <1%) and H impurities in the films. GIXRD patterns exhibited polycrystalline AlN and GaN thin films with (hexagonal) wurtzite crystal structure. Crystallite sizes were 19.2 and 24.8 nm for AlN, and 10.2 and 9.3 nm for GaN films deposited using NH_3 and N_2/H_2 plasma, respectively. The HR-TEM image of the GaN thin film deposited using NH_3 plasma further revealed the existence of relatively large crystals in the film, which can extend along the film thickness.

HCPA-ALD parameters were optimized at 200 °C for the deposition of AlN and GaN thin films. Trimethylmetal precursor and N_2/H_2 saturation curves evidenced the self-limiting growth of AlN and GaN at this temperature. AlN exhibited linear growth with a slight nucleation delay. The GPC of AlN was high; *i.e.* ~1.0 Å. In the case of GaN, the GPC decreased with the increasing number of deposition cycles, which indicates substrate-enhanced growth. The GPC was found to be 0.22 Å for the 900-cycle GaN deposition. 59.2 nm thick AlN and 20.1 nm thick GaN thin films deposited using optimized process parameters were characterized using SE, HR-XPS, GIXRD, XRR, and AFM. Refractive indices of AlN and GaN thin films were determined to be 1.94 and 2.17 at 632 nm, respectively, using the Cauchy dispersion function. Al 2p (Ga 3d) and N 1s HR-XPS spectra confirmed the metal nitride bonding states in AlN (GaN) films. The mass densities of AlN and GaN thin films were estimated to be 2.82 and 5.86 g cm^{-3} using XRR. Rms roughness values determined by XRR were higher than those directly measured using AFM; *i.e.* 1.97 and 0.64 nm for AlN and GaN thin films deposited on Si (100) substrates, respectively. Results of the depositions carried out using N_2 plasma have shown that this process results in low-quality films, and therefore is not eligible for the low-temperature deposition of AlN and GaN.

$Al_xGa_{1-x}N$ thin films were obtained *via* digital alloying, where the main HCPA-ALD cycle consisted of different numbers of AlN and GaN subcycles; *i.e.* AlN : GaN = 1 : 3, 1 : 1, and 3 : 1. Alloy compositions were determined by Vegard's rule to be 0.68 (AlN–GaN = 1 : 3), 0.95 (1 : 1), and 0.96 (3 : 1) using the *c* lattice parameters, which were roughly calculated from the (002) peak positions. The *c* lattice parameters of binary AlN and GaN thin films were also estimated and used for the calculations in order to minimize the errors that may arise due to the presence of strain in deposited films. Refractive index values of the $Al_xGa_{1-x}N$ thin films decreased from 2.03 to 1.96 as the Al content increased from 0.68 to 0.96. Transmissions of AlN, GaN, and $Al_xGa_{1-x}N$ thin films were equal to the substrate transmission (~93%) in the visible spectrum, indicating absorption-free films. Optical band edge values of the $Al_xGa_{1-x}N$ films shifted to lower wavelengths with increasing Al content, which confirms the adjustability of band edge values with compositional digital alloying.

Acknowledgements

This work was performed at UNAM – Institute of Materials Science and Nanotechnology, which is supported by the State Planning Organization of Turkey through the National Nanotechnology Research Center Project. The authors acknowledge Dr. S. Butcher (Meaglow Ltd.) for the helpful discussions and comments. C.O.-A. acknowledges TUBITAK-BIDEB for National PhD Fellowship. E.G. acknowledges the financial support from TUBITAK (BIDEB 2232, Project # 113C020). N.B. acknowledges support from Marie Curie International Reintegration Grant (NEMSmart, Grant # PIRG05-GA-2009-249196). A.K.O. and N.B. acknowledge the financial support from TUBITAK (Project # 112M004 and 112M482). M. Guler from UNAM is acknowledged for TEM sample preparation and HR-TEM imaging.

Notes and references

1 S. C. Jain, M. Willander, J. Narayan and R. Van Overstraeten, *J. Appl. Phys.*, 2000, **87**, 965.
2 J. Wu, *J. Appl. Phys.*, 2009, **106**, 011101.
3 Z. Chen, S. Newman, D. Brown, R. Chung, S. Keller, U. K. Mishra, S. P. Denbaars and S. Nakamura, *Appl. Phys. Lett.*, 2008, **93**, 191906.
4 M. Alevli, G. Durkaya, A. Weerasekara, A. G. U. Perera, N. Dietz, W. Fenwick, V. Woods and I. Ferguson, *Appl. Phys. Lett.*, 2006, **89**, 112119.
5 M. E. Lin, B. Sverdlov, G. L. Zhou and H. Morkoç, *Appl. Phys. Lett.*, 1993, **62**, 3479.
6 R. L. Puurunen, *J. Appl. Phys.*, 2005, **97**, 121301.
7 S. Y. Yang, G. Jeon and J. K. Kim, *J. Mater. Chem.*, 2012, **22**, 23017.
8 L. K. Tan, X. Liu and H. Gao, *J. Mater. Chem.*, 2011, **21**, 11084.
9 F. Kayaci, C. Ozgit-Akgun, N. Biyikli and T. Uyar, *RSC Adv.*, 2013, **3**, 6817.
10 J. Jokinen, P. Haussalo, J. Keinonen, M. Ritala, D. Riihelä and M. Leskelä, *Thin Solid Films*, 1996, **289**, 159.
11 J. N. Kidder, Jr, J. S. Kuo, A. Ludviksson, T. P. Pearsall, J. W. Rogers, Jr, J. M. Grant, L. R. Allen and S. T. Hsu, *J. Vac. Sci. Technol., A*, 1995, **13**, 711.
12 M. A. Khan, J. N. Kuznia, R. A. Skogman, D. T. Olson, M. Mac Millan and W. J. Choyke, *Appl. Phys. Lett.*, 1992, **61**, 2539.
13 D. Riihelä, M. Ritala, R. Matero, M. Leskelä, J. Jokinen and P. Haussalo, *Chem. Vap. Deposition*, 1996, **2**, 277.
14 H. Liu and J. W. Rogers, Jr, *J. Vac. Sci. Technol., A*, 1999, **17**, 325.
15 G. Liu, E. W. Deguns, L. Lecordier, G. Sundaram and J. S. Becker, *ECS Trans.*, 2011, **41**, 219.
16 Y. J. Lee and S.-W. Kang, *Thin Solid Films*, 2004, **446**, 227.
17 Y. J. Lee, *J. Cryst. Growth*, 2004, **266**, 568.
18 X. Liu, S. Ramanathan, E. Lee and T. E. Seidel, *Mater. Res. Soc. Symp. Proc.*, 2004, **811**, 11.
19 D. Eom, S. Y. No, C. S. Hwang and H. J. Kim, *J. Electrochem. Soc.*, 2006, **153**, C229.
20 K.-H. Kim, N.-W. Kwak and S. H. Lee, *Electron. Mater. Lett.*, 2009, **5**, 83.
21 C. Ozgit, I. Donmez, M. Alevli and N. Biyikli, *Thin Solid Films*, 2012, **520**, 2750.
22 M. Alevli, C. Ozgit, I. Donmez and N. Biyikli, *Phys. Status Solidi A*, 2012, **209**, 266.
23 M. Alevli, C. Ozgit, I. Donmez and N. Biyikli, *J. Cryst. Growth*, 2011, **335**, 51.
24 M. Bosund, T. Sajavaara, M. Laitinen, T. Huhtio, M. Putkonen, V.-M. Airaksinen and H. Lipsanen, *Appl. Surf. Sci.*, 2011, **257**, 7827.
25 Y.-R. Shin, W.-S. Kwack, Y. C. Park, J.-H. Kim, S.-Y. Shin, K. I. Moon, H.-W. Lee and S.-H. Kwon, *Mater. Res. Bull.*, 2012, **47**, 790.
26 W. Lei and Q. Chen, *J. Vac. Sci. Technol., A*, 2013, **31**, 01A114.
27 A. P. Perros, H. Hakola, T. Sajavaara, T. Huhtio and H. Lipsanen, *J. Phys. D: Appl. Phys.*, 2013, **46**, 505502.

28 N. Nepal, S. B. Qadri, J. K. Hite, N. A. Mahadik, M. A. Mastro and C. R. Eddy, Jr, *Appl. Phys. Lett.*, 2013, **103**, 082110.
29 B. J. Choi, J. J. Yang, M.-X. Zhang, K. J. Norris, D. A. A. Ohlberg, N. P. Kobayashi, G. Medeiros-Ribeiro and R. S. Williams, *Appl. Phys. A: Mater. Sci. Process.*, 2012, **109**, 1.
30 Z. Tang, S. Huang, Q. Jiang, S. Liu, C. Liu and K. J. Chen, *IEEE Electron Device Lett.*, 2013, **34**, 366.
31 C. Liu, S. Liu, S. Huang and K. J. Chen, *IEEE Electron Device Lett.*, 2013, **34**, 1106.
32 A. D. Koehler, N. Nepal, T. J. Anderson, M. J. Tadjer, K. D. Hobart, C. R. Eddy, Jr and F. J. Kub, *IEEE Electron Device Lett.*, 2013, **34**, 1115.
33 Y.-H. Hwang, L. Liu, C. Velez, F. Ren, B. P. Gila, D. Hays, S. J. Pearton, E. Lambers, I. I. Kravchenko, C.-F. Lo and J. W. Johnson, *J. Vac. Sci. Technol., B: Microelectron. Nanometer Struct.–Process., Meas., Phenom.*, 2013, **31**, 052201.
34 C.-P. Lu, M. Schmidt, H. D. B. Gottlob and H. Kurz, *Proceedings of 2010 International Symposium on VLSI Technology, System and Application*, Taiwan, 2010.
35 M. Bosund, P. Mattila, A. Aierken, T. Hakkarainen, H. Koskenvaara, M. Sopanen, V.-M. Airaksinen and H. Lipsanen, *Appl. Surf. Sci.*, 2010, **256**, 7434.
36 H. Jussila, P. Mattila, J. Oksanen, A. Perros, J. Riikonen, M. Bosund, A. Varpula, T. Huhtio, H. Lipsanen and M. Sopanen, *Appl. Phys. Lett.*, 2012, **100**, 071606.
37 S. Huang, K. Wei, Z. Tang, S. Yang, C. Liu, L. Guo, B. Shen, J. Zhang, X. Kong, G. Liu, Y. Zheng, X. Liu and K. J. Chen, *J. Appl. Phys.*, 2013, **114**, 144509.
38 M. A. Khan, R. A. Skogman, J. M. Van Hove, D. T. Olson and J. N. Kuznia, *Appl. Phys. Lett.*, 1992, **60**, 1366.
39 N. H. Karam, T. Parodos, P. Colter, D. McNulty, W. Rowland, J. Schetzina, N. El-Masry and S. M. Bedair, *Appl. Phys. Lett.*, 1995, **67**, 94.
40 C.-Y. Hwang, P. Lu, W. E. Mayo, Y. Lut and H. Liut, *Mater. Res. Soc. Symp. Proc.*, 1994, **326**, 347.
41 H. Tsuchiya, M. Akamatsu, M. Ishida and F. Hasegawa, *Jpn. J. Appl. Phys.*, 1996, **35**, L748.
42 O. H. Kim, D. Kim and T. Anderson, *J. Vac. Sci. Technol., A*, 2009, **27**, 923.
43 A. Koukitu, Y. Kumagai, T. Taki and H. Seki, *Jpn. J. Appl. Phys.*, 1999, **38**, 4980.
44 J. Sumakeris, Z. Sitar, K. S. Ailey-Trent, K. L. More and R. F. Davis, *Thin Solid Films*, 1993, **225**, 244.
45 T. R. Sharp, A. K. Peter, C. J. Hodson, B. MacKenzie, C. Pugh, M. Loveday and R. Gunn, *Presented in part at the 13th International Conference on Atomic Layer Deposition*, San Diego, July 2013.
46 C. Ozgit, I. Donmez, M. Alevli and N. Biyikli, *J. Vac. Sci. Technol., A*, 2012, **30**, 01A124.
47 C. Ozgit, I. Donmez, M. Alevli and N. Biyikli, *Acta Phys. Pol., A*, 2012, **120**, A-55.
48 K. S. A. Butcher, Afifuddin, P. P.-T. Chen and T. L. Tansley, *Phys. Status Solidi C*, 2002, **0**, 156.
49 C. Ozgit-Akgun, I. Donmez and N. Biyikli, *ECS Trans.*, 2013, **58**, 289.
50 L. Bárdoš, *Surf. Coat. Technol.*, 1996, **86–87**, 648.
51 K. S. A. Butcher, B. W. Kemp, I. B. Hristov, P. Terziyska, P. W. Binsted and D. Alexandrov, *Jpn. J. Appl. Phys.*, 2012, **51**, 01AF02.
52 H. C. Barshilia, B. Deepthi and K. S. Rajam, *Thin Solid Films*, 2008, **516**, 4168.
53 G. Yu, G. Wang, H. Ishikawa, M. Umeno, T. Soga, T. Egawa, J. Watanabe and T. Jimbo, *Appl. Phys. Lett.*, 1997, **70**, 3209.
54 K. S. A. Butcher, T. L. Tansley and X. Li, *Surf. Interface Anal.*, 1997, **25**, 99.
55 K. S. A. Butcher, Afifuddin, T. L. Tansley, N. Brack, P. J. Pigram, H. Timmers, K. E. Prince and R. G. Elliman, *Appl. Surf. Sci.*, 2004, **230**, 18.
56 J. Mayer, L. A. Giannuzzi, T. Kamino and J. Michael, *MRS Bull.*, 2007, **32**, 400.
57 D. Manova, V. Dimitrova, W. Fukarek and D. Karpuzov, *Surf. Coat. Technol.*, 1998, **106**, 205.
58 L. Rosenberger, R. Baird, E. McCullen, G. Auner and G. Shreve, *Surf. Interface Anal.*, 2008, **40**, 1254.
59 H. M. Liao, R. N. S. Sodhi and T. W. Coyle, *J. Vac. Sci. Technol., A*, 1993, **11**, 2681.
60 S. D. Wolter, B. P. Luther, D. L. Waltemyer, C. Önneby and S. E. Mohney, *Appl. Phys. Lett.*, 1997, **70**, 2156.
61 V. Matolín, S. Fabík, J. Glosík, L. Bideux, Y. Ould-Metidji and B. Gruzza, *Vacuum*, 2004, **76**, 471.
62 P. Kumar, M. Kumar, Govind, B. R. Mehta and S. M. Shivaprasad, *Appl. Surf. Sci.*, 2009, **256**, 517.
63 W. R. L. Lambrecht, B. Segall, S. Strite, G. Martin, A. Agarwal, H. Morkoç and A. Rockett, *Phys. Rev. B: Condens. Matter Mater. Phys.*, 1994, **50**, 14155.
64 Z. Majlinger, A. Bozanic, M. Petravic, K.-J. Kim, B. Kim and Y.-W. Yang, *Vacuum*, 2010, **84**, 41.
65 G. Moldovan, I. Harrison, M. Roe and P. D. Brown, *Inst. Phys. Conf. Ser.*, 2004, **179**, 115.
66 R. Carin, J. P. Deville and J. Werckmann, *Surf. Interface Anal.*, 1990, **16**, 65.
67 M. E. Levinshtein, S. L. Rumyantsev, and M. S. Shur, in *Properties of Advanced Semiconductor Materials*, ed. M. E. Levinshtein, S. L. Rumyantsev and M. S. Shur, Wiley, New York, 1st edn, 2001, ch. 1, p. 1, ch. 2, p. 31.
68 M. A. Moram and M. E. Vickers, *Rep. Prog. Phys.*, 2009, **72**, 036502.
69 W. Rindner and E. Pittelli, *J. Appl. Phys.*, 1966, **37**, 4437.
70 N. Preschilla, A. S. Major, N. Kumar, I. Samajdar and R. S. Srinivasa, *Appl. Phys. Lett.*, 2000, **77**, 1861.

